

Exciton coupling in molecular salts of 2-(1,8-naphthalimido)ethanoic acid and cyclic amines: modulation of the solid-state luminescence†

Cite this: *CrystEngComm*, 2013, 15, 10470

Simone d'Agostino,^a Fabrizia Grepioni,^{*a} Dario Braga,^a Daniele Moreschi,^a Valeria Fattori,^b Francesca Delchiaro,^a Simone Di Motta^a and Fabrizia Negri^{*a}

In this study we have purposely altered the solid state luminescence properties of 2-(1,8-naphthalimido)ethanoic acid (NEaH) (**0**) *via* molecular salts formation with cyclic amines such as 1,4-diazabicyclo[2.2.2]octane (DABCO), quinuclidine (ABCO), 3-quinuclidinol (OH-ABCO), and piperazine (PIP). All crystalline materials have been characterized in the solid state *via* single-crystal and variable temperature powder X-ray diffraction and thermal methods; luminescence spectra in the solid state have been recorded. Exciton interactions have been determined with quantum-chemical calculations for all molecular organic salts, and tuning of their magnitude in response to changes in the crystal packing has been demonstrated. It is suggested that the variations in photoluminescence can be interpreted on the basis of the different excitonic interactions amongst the naphthalimide moieties.

Received 4th July 2013,
Accepted 9th October 2013

DOI: 10.1039/c3ce41651h

www.rsc.org/crystengcomm

Introduction

Crystal engineering¹ is aimed to the design and preparation of crystalline materials with desired properties, starting from a knowledge of the supramolecular bonding capacity of molecular components that self-assemble in the solid. Multi-component crystals, such as co-crystals and molecular salts, are attracting much interest because of the potential new solid state properties deriving from a combination of molecular components with the structure of the final supramolecular aggregate. Excellent examples can be found in solid state templated photoreactions² or in cases where Active Pharmaceutical Ingredients (APIs) are turned into multiple crystal forms such as co-crystals, ionic co-crystals, coordination compounds and molecular salts to improve properties such as thermal stability, morphology, dissolution rate, *etc.*³ Most recently there has been a surge of interest in the use of co-crystals as a means to modify fluorescence⁴ and phosphorescence⁵ properties of emitting molecules such as organic dyes.⁶ Solid state luminescent materials are of great interest and are studied for their potential applications in the field of optoelectronic devices.⁷ Among them, N-substituted naphthalimides derivatives are an attractive class of organic

dyes.⁶ Their photophysical properties are useful in many applications as organic light-emitting diodes,⁸ fluorescent dyes for polymers and textile materials,^{6,9} but also as sensors, liquid crystals displays, and logic gates.¹⁰ It has been recently reported that 2-(1,8-naphthalimido)ethanoic acid (NEaH) exhibits a blue fluorescence in the solid state.¹¹

In this work 2-(1,8-naphthalimido)ethanoic acid NEaH, chosen as the starting photoactive component, has been reacted with the cyclic amines reported in Scheme 1: the organic bases were chosen with the aim of purposely altering the exciton interactions, therefore the luminescent properties of the resulting crystalline material, by altering the packing pattern of the NEaH chromophore. Beside the tuning of exciton interactions also the tendency to form excimers, already known for NEaH derivatives, may be affected by packing and can therefore influence the photoluminescence. In view of our successful experience with the use of mechanochemical methods,¹² all crystalline materials were prepared *via* kneading,^{12a} *i.e.* grinding of the starting materials in the presence of a catalytic amount of solvent.

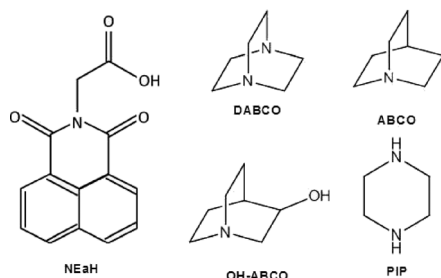
Results and discussion

For the purpose of this study (NEaH) was mechanically reacted with each aliphatic base (DABCO, ABCO, OH-ABCO, and PIP) in the presence of a catalytic amount of solvent (kneading), under a UV lamp (365 nm). When the samples were kneaded in the presence of water, a change in the luminescence colour was noticed. The blue luminescence of NEaH (**0**) changed to violet when the solid was kneaded in the presence of half an equivalent of 1,4-diazabicyclo[2.2.2]octane

^a Dipartimento di Chimica "G. Ciamician", Università di Bologna, Via Selmi 2, 40126 Bologna, Italy. E-mail: fabrizia.grepioni@unibo.it, fabrizia.negri@unibo.it

^b Istituto per la Sintesi Organica e la Fotoreattività (ISOF) – CNR, Via Gobetti 101, 40129 Bologna, Italy

† Electronic supplementary information (ESI) available: Solid-state structural characterization, DSC and TGA, computational details. CCDC 941379–941382. For ESI and crystallographic data in CIF or other electronic format see DOI: 10.1039/c3ce41651h



Scheme 1 The photoactive component, 2-(1,8-naphthalimido)ethanoic acid (NEaH), and the bases utilized in the present study: 1,4-diazabicyclo[2.2.2]octane (DABCO), quinuclidine (ABCO), 3-quinuclidinol (OH-ABCO), and piperazine (PIP).

(DABCO) or piperazine (PIP), and to green when kneading was carried out in the presence of one equivalent of quinuclidine (ABCO) or 3-quinuclidinol (OH-ABCO) (see Table 1).

The formation of new crystal forms (see Table 1) was confirmed by comparing X-ray powder diffraction patterns of the solid products with those calculated on the basis of single crystals of the corresponding compounds, obtained *via* recrystallization from solution[‡] (see Fig. S1[†]). Under irradiation with a suitable UV lamp ($\lambda = 365$ nm) the crystals obtained from solution exhibited the same luminescence colours of the corresponding solid–solid reaction products (see Fig. 1).

The structure of NEaH (**0**) was reported recently, and for its description the reader is addressed to reference.¹¹ Single crystal X-ray diffraction shows that all compounds are in the form of molecular salts containing completely deprotonated 2-(1,8-naphthalimido)ethanoate anions and, depending on the number of N-atoms on the base used as a reagent, mono/di-protonated cations. The reaction with DABCO yields the anhydrous form $[\text{DABCOH}_2][\text{NEa}]_2$ (**1**) constituted of discrete units held together by hydrogen bonds between a fully protonated DABCO unit, hence in the form of the dication DABCOH_2^{2+} , and the carboxylate groups on the deprotonated NEa^- units. The hydrogen bonding distance is typical of a “charge assisted” hydrogen bond [$\text{O}_\text{O}^- \cdots \text{O}_\text{N-H}^+ = 2.534(2)$ Å], see Fig. 2.¹³

The discrete, overall neutral trimeric units interact *via* π -stacking and are organized in zig-zag ribbons in the crystal. Adjacent ribbons form 2D-layers parallel to the *ac*-plane (see Fig. 3a); a second layer is shifted with respect to the first (see blue spheres in Fig. 3b) and is accommodated in the empty cavities of the first layer.

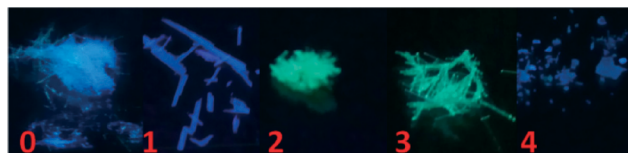


Fig. 1 Pictures, taken under UV light (365 nm), of fluorescent crystals of pure [NEaH] (**0**) and of the molecular salts $[\text{DABCOH}_2][\text{NEa}]_2$ (**1**), $[\text{ABCOH}][\text{NEa}]\cdot 4\text{H}_2\text{O}$ (**2**), $[\text{OH-ABCOH}][\text{NEa}]\cdot 1.5\text{H}_2\text{O}$ (**3**) and $[\text{PIPH}_2][\text{NEa}]_2\cdot 4\text{H}_2\text{O}$ (**4**), obtained *via* recrystallization from solution.

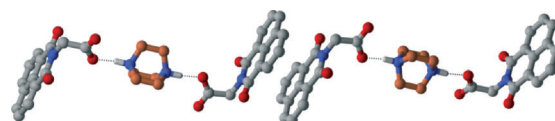


Fig. 2 Discrete hydrogen bonded units in crystalline $[\text{DABCOH}_2][\text{NEa}]_2$ (**1**). H_CH omitted for clarity.

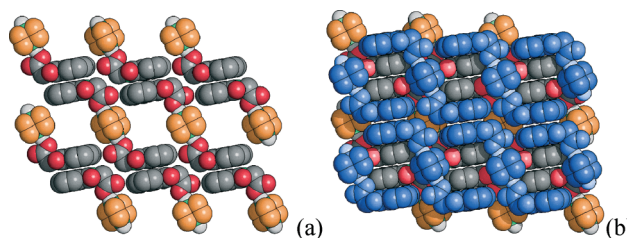


Fig. 3 A 2D-layer of π -stacked hydrogen bonded trimeric units in crystalline **1** (a); a second layer (in blue) fills in the voids (b). H_CH atoms not shown for clarity.

The reaction between NEaH and ABCO also yields a molecular salt *via* proton transfer from acid to base; the product is a tetrahydrate, of formula $[\text{ABCOH}][\text{NEa}]\cdot 4\text{H}_2\text{O}$ (**2**). The water molecules are organized in hydrogen bonded hexamers, sharing two opposite edges with adjacent rings, thus forming an infinite tape [T6(2) motif,¹⁴ $\text{O}_\text{w} \cdots \text{O}_\text{w} = 2.7509(2) - 2.829(2)$ Å, $\text{O}_\text{w} \cdots \text{O}_\text{w} \cdots \text{O}_\text{w}$ angles = $115.62(9) - 126.5(1)^\circ$]; the angle between the planes defined by the hexamers is of *ca.* 127 deg. The water hexamers, in turn, interact through a net of hydrogen bonds with the $[\text{NEa}]^-$ anions [$\text{O}_\text{w} \cdots \text{O}_\text{C}=\text{O}/\text{C}-\text{O}^- = 2.718(2) - 2.720(3)$ Å] and with the $[\text{ABCOH}]^+$ cations [$\text{O}_\text{w} \cdots \text{N}_\text{N-H}^+ = 2.672(3)$ Å] (see Fig. 4).

Differently from what observed in crystalline **1**, no close contact is observed between cation and anion; all interactions between the two moieties are mediated by the water molecules, which act as a “neutral glue”, thus forming a layer

Table 1 List of the solid compounds discussed in this study

Compound	Code	Fluorescence colour ^a (UV-lamp, $\lambda = 365$ nm)
NEaH ^b	0	Blue
$[\text{DABCOH}_2][\text{NEa}]_2$	1	Violet
$[\text{ABCOH}][\text{NEa}]\cdot 4\text{H}_2\text{O}$	2	Green
$[\text{OH-ABCOH}][\text{NEa}]\cdot 1.5\text{H}_2\text{O}$	3	Green
$[\text{PIPH}_2][\text{NEa}]_2\cdot 4\text{H}_2\text{O}$	4	Violet

^a All compounds are colourless under visible light. ^b Known structure¹¹ (CSD refcode: UBAGOV).

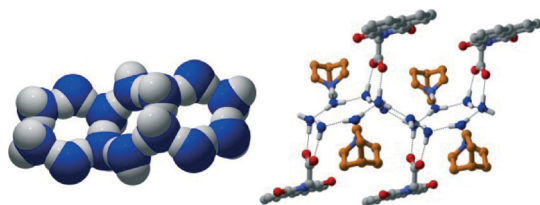


Fig. 4 (Left) Space filling representation of the T6(2) water motif in crystalline **2**; (right) water hexamers interacting through hydrogen bonds with the $[\text{NEa}]^-$ anions and with the $[\text{ABCOH}]^+$ cations. H_{CH} omitted for clarity.

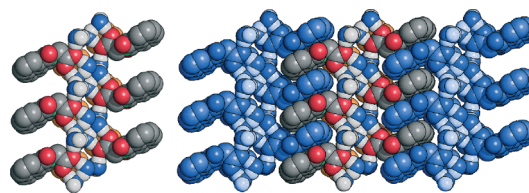


Fig. 5 (Left) Side view, along the b -axis, of the hydrogen-bonded layer extending parallel to the ab -plane in crystalline **2**, with anions and cations “glued” together *via* the water hexamers; (right) on both sides, additional layers (in blue) “click” to the central one *via* π -stacking interactions. H_{CH} atoms not shown for clarity.

extending parallel to the ab -plane. The aromatic moieties stick out of the layer (see Fig. 5, left); two adjacent layers “click” to the central one *via* π -stacking interactions (see Fig. 5, right).

The reaction of NEaH with OH-ABCO also yields a hydrated phase of formula $[\text{OH-ABCOH}][\text{NEa}]\cdot 1.5\text{H}_2\text{O}$ (**3**). Through the carboxylate function the $[\text{NEa}]^-$ anions interact with both the protonated N-atom and the hydroxyl group on the $[\text{OH-ABCOH}]^+$ cationic units [$\text{O}_{\text{COO}^-}\cdots\text{N}_{\text{N-H}^+} = 2.668(7)$ – $2.691(8)$ Å; $\text{O}_{\text{COO}^-}\cdots\text{O}_{\text{OH}} = 2.775(7)$ Å, see Fig. 6], which in turn also interact with water molecules [$\text{O}_{\text{OH}}\cdots\text{O}_{\text{w}} = 2.756(8)$ – $2.892(9)$ Å, not shown in the picture]. $[\text{NEa}]^-$ anions interact also with water molecule by using either the carboxylate and the imido carbonyl group [$\text{O}_{\text{COO}^-}\cdots\text{O}_{\text{w}} = 2.728(9)$ – $2.825(8)$ Å; $\text{O}_{\text{CO}}\cdots\text{O}_{\text{w}} = 2.871(1)$ Å]. The water molecules interact with each other *via* hydrogen bonds, forming trimeric units [$\text{O}_{\text{w}}\cdots\text{O}_{\text{w}} = 2.90(1)$ – $2.72(1)$ Å, see Fig. 6]. The resulting packing is reminiscent of the one observed in crystalline **2**, with adjacent layers forming π -stacking interactions *via* interpenetration of the aromatic moieties, in a velcro-like fashion (see Fig. 7).

In crystalline $[\text{PIPH}_2][\text{NEa}]_2\cdot 4\text{H}_2\text{O}$ (**4**) there is a complex network of hydrogen bonding interactions between the carboxylate function on the $[\text{NEa}]^-$ anions and the water molecules [$\text{O}_{\text{w}}\cdots\text{O}_{\text{C-O}^-} = 2.747(4)$ – $2.988(4)$ Å] and the $[\text{PIPH}_2]^{2+}$ dication [$\text{O}_{\text{w}}\cdots\text{N}_{\text{N-H}^+} = 2.746(4)$ Å], which in turn interacts with the imide carbonyl [$\text{O}_{\text{C=O}}\cdots\text{N}_{\text{N-H}^+} = 2.795(4)$ Å] (see Fig. 8). The water molecules also interact with each other *via* dimer formation [$\text{O}_{\text{w}}\cdots\text{O}_{\text{w}} = 2.90(1)$ – $2.749(4)$ Å] (see Fig. 8).

The packing of crystalline **4** markedly differs from those described above, in that no π -stacking interactions are at work in this solid: the aromatic units are arranged in a herring-bone fashion, as can easily be seen in Fig. 9.

Since the solid state photophysical behavior depends strongly on the interactions between the chromophores, it is important to see if the organization of the molecular ions in the solid state has led to any recognizable pattern in the crystal packings and if these reflect to any extent on the properties. The focus is on patterns involving π -stacking, as these are more relevant to photophysical properties. (Of course this does not necessarily imply that these are the most relevant in keeping the crystal together, *i.e.* the most relevant in terms of

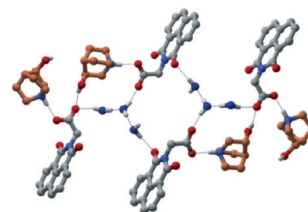


Fig. 6 Hydrogen bonding interactions in crystalline $[(\text{NEa})(\text{OH-ABCOH})\cdot 1.5\text{H}_2\text{O}]$ (**3**). H_{CH} atoms not shown for clarity.

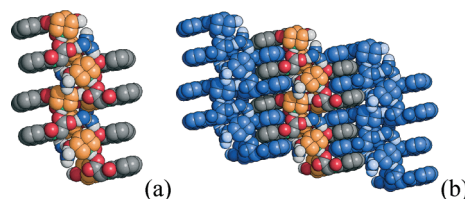


Fig. 7 (a) A layer (side-view) of hydrogen bonded cations, anions and water molecules in crystalline **3**; (b) on both sides, additional layers (in blue) are linked to the central one *via* π -stacking interactions.

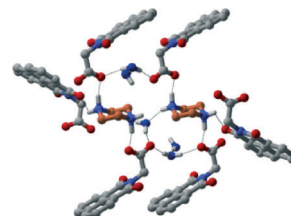


Fig. 8 Hydrogen bonding interactions in crystalline $[\text{PIPH}_2][\text{NEa}]_2\cdot 4\text{H}_2\text{O}$ (**4**). H_{CH} atoms not shown for clarity.

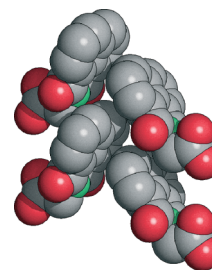


Fig. 9 Van der Waals spheres representation of the herring-bone arrangement of the aromatic units in crystalline **4**. H_{CH} atoms not shown for clarity.

‡ All solvents and chemicals were bought from Sigma-Aldrich and used without further purification; doubly-distilled water was used.

energy, as in crystals made of molecular ions interactions can still be fairly energetic at large distances).

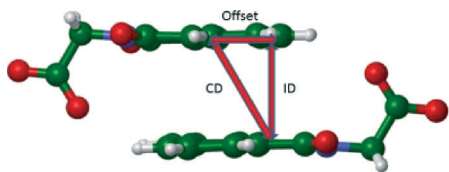
Scheme 2 shows how geometrical parameters were evaluated for the “dimers” present in the solids; calculated values for all compounds are reported in Table 2, together with graphical representation of all relevant dimers also used for the computational investigation. For compounds 1–3 the naphthalimide moieties are oriented parallel to each other in a columnar fashion; different π -stacking modes are detected. Crystalline 4 differs from the other solids, as an edge-to-face interaction is at work between the naphthalimide moieties (see Fig. 9 and Table 2).

Thermal behaviour

Thermal behaviour of the hydrated compounds 2, 3 and 4 was also investigated, in order to detect a possible additional effect on luminescence colour change due to water removal from the crystal lattice. Thermal gravimetric analysis for compound [ABCOH][NEa] \cdot 4H₂O (2) indicates a weight loss of 15.6% in the range 37–100 °C, corresponding to the release of 4 water molecules per formula unit. The DSC trace shows an endothermic peak at 65 °C (peak temperature, $\Delta H = 310.51 \text{ J mol}^{-1}$) in the same region (see Fig. S2†).

Variable temperature powder diffraction experiments were particularly useful to investigate the dehydration processes (see Fig. 10a). Formation of a crystalline anhydrous phase (2_ahyd) following dehydration is observed upon heating a polycrystalline sample of 2 up to 100 °C. The transformation is fully reversible: when the sample is cooled back to room temperature, 2_ahyd reverts back to the starting solid 2 *via* water uptake from the atmosphere (this process is accelerated if the powder sample is ground).

In the case of compound [OH-ABCOH][NEa] \cdot 1.5H₂O (3) the thermogram indicates a weight loss of 7.2% in the range 35–110 °C, consistent with the release of 1.5 water molecules per formula unit. The DSC trace shows an endothermic peak at 69 °C (peak temperature, $\Delta H = 113 \text{ J mol}^{-1}$) in the same interval (see Fig. S3†). The dehydration process was also followed with variable temperature powder diffraction (Fig. 10b). Heating a sample up to 120 °C results in the transformation to an anhydrous phase (3_ahyd). As observed with compound 2, the change is fully reversible, and after cooling back to room temperature 3_ahyd reverts back to the starting solid 3 *via* water uptake from the atmosphere; again, the process is accelerated if the powder is ground.



Scheme 2 ID = interplanar distance; CD = distance between the geometrical centres of the aromatic systems; offset = shift of the geometrical centres, in projection.

Table 2 Types of dimers observed in crystalline 1–4, together with their relevant geometrical parameters and codes used for the computational study

Compound and dimer	Side view	Top view
(1) DIMER A ID = 3.45 Å CD = 3.62 offset = 1.09 Å		
(1) DIMER B ID = 3.12 Å CD = 6.31 Å offset = 5.49 Å		
(1) DIMER C ID = 3.31 Å CD = 4.99 Å offset = 3.73 Å		
(2) DIMER A ID = 3.66 Å CD = 3.92 Å offset = 1.40 Å		
(2) DIMER B ID = 3.52 Å CD = 4.57 Å offset = 2.92 Å		
(3) ID = 3.46 Å CD = 3.84 Å offset = 1.67 Å		
(4) $d_{C-H \cdots \pi} = 2.69\text{--}3.44 \text{ Å}$ or $d_{C \cdots \pi} = 3.51\text{--}4.06 \text{ Å}$		

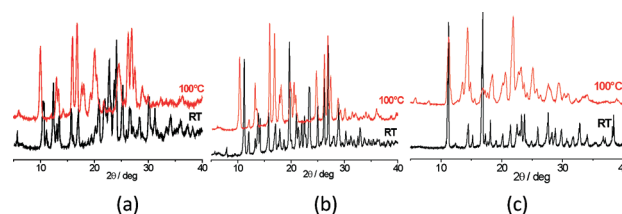


Fig. 10 Comparison of the experimental VT-XRPD patterns for the hydrated phase at RT (black) and the anhydrous phase at 100 °C (red) for crystalline 2 (a), 3 (b) and 4 (c).

An analogous behavior can be observed for crystalline [PIPH₂][NEa]₂ \cdot 4H₂O (4). A TGA trace indicates a weight loss of 11% in the range 50–100 °C, due to the release of 4 water molecules per formula unit. The anhydrous phase is stable up to *ca.* 200 °C, then decomposition is observed. The DSC trace shows an endothermic peak at 79 °C (peak temperature, $\Delta H = 243 \text{ J mol}^{-1}$) (see Fig. S4†). Variable temperature powder diffraction experiments for this compound are presented in Fig. 10c. Heating up to 100 °C results in the formation of a

new anhydrous phase, denoted as **4_anhyd**. Even in this case, when the sample is cooled back to room temperature, the anhydrous phase reverts to the starting solid (**4**) *via* water uptake from atmospheric moisture; as noted for the previous systems, the process is accelerated *via* grinding.

For compounds **2**, **3**, and **4** no apparent colour changes, under day light or UV light (365 nm), have been detected during or after dehydration at high temperature. Unfortunately, it was not possible to carry out photophysical measurements on the anhydrous phases **2_anhyd**, **3_anhyd**, and **4_anhyd**, because upon cooling to room temperature they rapidly reverted to their hydrated forms.

Photophysics

We examined the optical properties of NEaH (**0**) in solution and in the solid state, and the luminescence properties of the crystalline materials [DABCOH₂][NEa]₂ (**1**), [ABCOH][NEa]·4H₂O (**2**), [OH-ABCOH][NEa]·1.5H₂O (**3**), and [PIPH₂][NEa]₂·4H₂O (**4**).

Electronic absorption spectra for NEaH (**0**) were recorded in methanol and dichloromethane solutions (Fig. 11a), and, as expected from previous solution studies of substituted 1,8-naphthalimides,¹⁵ the spectra show two absorption maxima, one at *ca.* 230 nm ($\lambda_{\text{max}} = 232 \text{ nm}$, $\epsilon = 55\,000 \text{ M}^{-1} \text{ cm}^{-1}$ and $\lambda_{\text{max}} = 236 \text{ nm}$, $\epsilon = 38\,000 \text{ M}^{-1} \text{ cm}^{-1}$ in methanol and

dichloromethane, respectively) and the second at *ca.* 330 nm ($\lambda_{\text{max}} = 333 \text{ nm}$, $\epsilon = 16\,900 \text{ M}^{-1} \text{ cm}^{-1}$ and $\lambda_{\text{max}} = 335 \text{ nm}$, $\epsilon = 11\,000 \text{ M}^{-1} \text{ cm}^{-1}$ in methanol and dichloromethane, respectively). Fig. 11b shows the fluorescence spectra of NEaH (**0**). As the excitation wavelengths we choose the maximum absorption wavelengths at 330 nm. In dichloromethane the compound shows a structured band with a maximum at 385 nm ($\Phi_{\text{em}} = 0.19$), while in methanol the same band is less resolved and slightly red-shifted, with a maximum at 387 nm ($\Phi_{\text{em}} = 0.075$).¹⁶ The methanol solution shows both a blue shifted absorption and a red shifted emission resulting in a slightly increased Stokes shift with respect to the dichloromethane solution, together with structure burring of the emission band and luminescence quenching. These effects can be associated to hydrogen bonding with the protic solvent. The electronic transitions from the singlet excited electronic state in 1,8-naphthalimide derivatives are affected by a triplet state very close in energy and having n,π^* character,¹⁷ therefore, the interactions of the carbonyl with a protic solvent affect the inter-system crossing processes and non-radiative deactivations.¹⁸

Photoluminescence spectra recorded on polycrystalline samples of NEaH (**0**), [DABCOH₂][NEa]₂ (**1**), [ABCOH][NEa]·4H₂O (**2**), [OH-ABCOH][NEa]·1.5H₂O (**3**), and [PIPH₂][NEa]₂·4H₂O (**4**) together with excitation spectra are shown in Fig. 12. Emission and excitation maxima for all samples are reported in Table 3 together with the wavelengths chosen as excitation and fluorescence quantum yields.

For all compounds both luminescence and excitation spectra are red-shifted compared to solution, while no effects of hypo/hyperchromism are present in the solid state (luminescence quantum yields are of the same order of magnitude in solution and in the solid state). Clearly, the spectral features in compounds (**0**)–(**4**) arise from the different intermolecular excitonic, van der Waals and π – π interactions at work in their crystals between the naphthalimide moieties, that stabilize the extended excited state (exciton), more than the ground state.^{11,19}

While the excitation spectra are relatively similar for all the compounds (all of them have a maximum or shoulder in the 385–390 nm range), the emission spectra clearly show distinct behaviours. The large differences in emission spectra and their marked red shift seem to indicate the presence of excimeric emission, which has been already reported for naphthalimide derivatives,²⁰ originated by the face-to-face interaction between two naphthalimide moieties.

Quantum-chemical modelling

The observed photophysical changes of the crystals result from the interplay of intramolecular vibronic activity, intermolecular interactions, among which excitonic interactions²¹ play a relevant role.

To investigate the modulation of exciton couplings induced by the different crystal packing and to discuss their possible influence on the photophysics we carried out

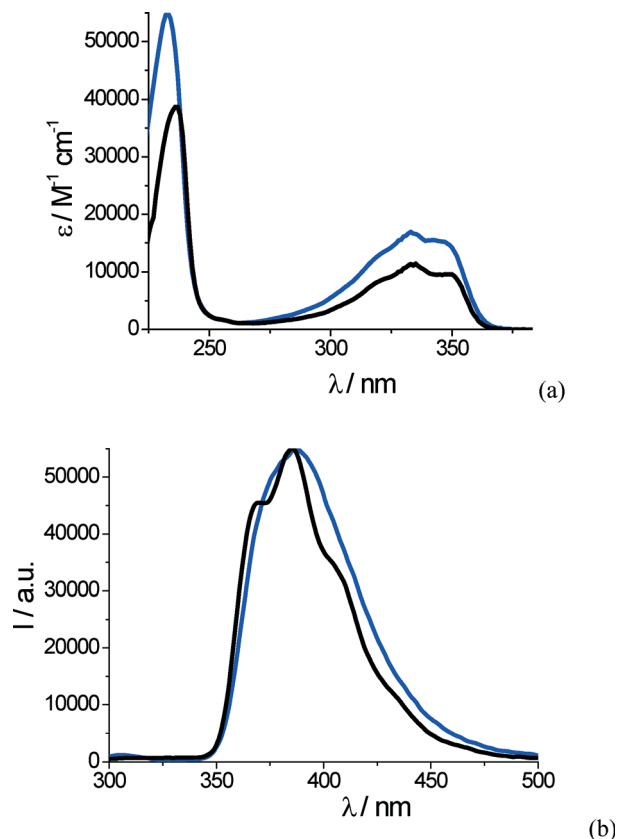


Fig. 11 (a) Electronic absorption spectra of NEaH (**0**) in methanol (blue) and dichloromethane (black) solution, and (b) normalized fluorescence spectra of NEaH (**0**) in methanol (blue) and dichloromethane (black) solution.

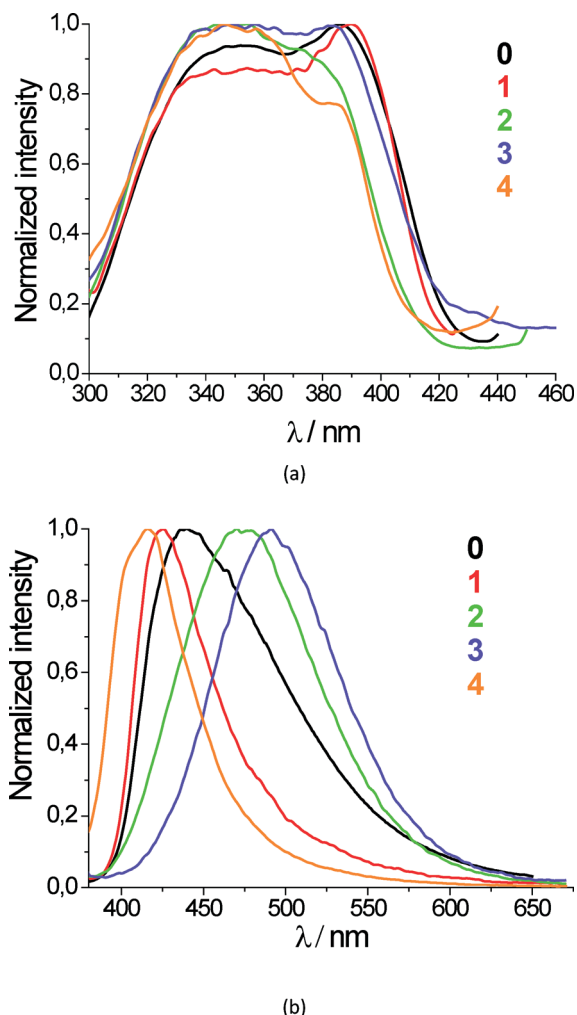


Fig. 12 (a) Normalized solid state excitation spectra recorded at RT for compounds 0, 1, 2, 3, and 4; (b) normalized solid state luminescence spectra recorded at RT for compounds 0, 1, 2, 3, and 4.

quantum-chemical calculations on the chromophores of compounds 0, 1 and 2. We first considered the isolated chromophore NEaH and evaluated the Stokes Shift (SS) between absorption and emission. To this end we determined the reorganization energies associated with relaxation in the ground and excited electronic states, within the adiabatic potential (AP) approach²² as schematically shown in Fig. 13.

The equilibrium structure of the ground and excited states were determined and the four energy values, indicated in Fig. S5[†] and collected in Table S1,[†] were employed to evaluate reorganization energies. The computed SS, sum of the two

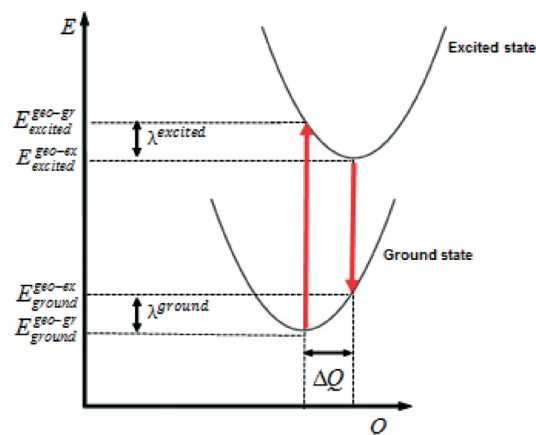


Fig. 13 Schematic representation of the potential energy surfaces for the ground and excited states of NEaH, showing the vertical absorption and emission transitions (red arrows), the normal mode displacement ΔQ , and the relaxation energies λ^{excited} and λ^{ground} .

reorganization energy values in Table S1,[†] amounts to 0.36 eV (0.52 eV) at B3LYP/6-31+G* (CAM-B3LYP/6-31+G*) and compares well with the experimental measurements in dichloromethane shown in Fig. 13 (*ca.* 0.48 eV) and with the data from literature for similar systems.

Different crystal packing may lead to different patterns of excitonic interactions. Therefore we identified the most relevant pairs of interacting chromophores (hereafter indicated as dimers) for some of the investigated crystals (compounds 0–2) and evaluated the excitonic couplings.

The dimers were determined by analyzing portions of crystals and selecting the relevant dimers according to the intermolecular distances between centers of mass. This procedure, already employed to investigate charge transport properties of crystalline organic semiconductors^{2,3} shows that there are two relevant dimers for 0, three for 1, and two for 2, whose center of mass distances are shorter than 7 Å. A summary of distances, orientations of the molecules in the dimers and labelling of the dimers are collected in Table S2,[†] Table 2 (for compounds 1 and 2) and Fig. S6[†] for compound 0.

Under the assumption that the excited states of molecular aggregates are weakly influenced by inter-molecular forces, they can be approximated by a linear combination of the excited states localized on the isolated molecule. Considering a simple dimer formed by two identical molecules, due to the presence of the V^{exciton} term, the localized excited states of the isolated molecules give rise to two delocalized excitonic states (Frenkel states) for the dimer, which are in phase (state

Table 3 Emission and excitation maxima and photoluminescence quantum yields in the solid state for the hydrated compounds 0, 1, 2, 3, and 4

Compound	λ_{ex} (nm)	λ_{em} (nm)	Φ_{em}	Fluorescence colour ($\lambda = 365$ nm)
NEaH (0)	386	440	0.13	Blue
[DABCOH ₂][NEa] ₂ (1)	390	425	0.11	Violet
[ABCOH][NEa]·4H ₂ O (2)	346	470	0.14	Green
[OH-ABCOH][NEa]·1.5H ₂ O (3)	357	491	0.13	Green
[PIPH ₂][NEa] ₂ ·4H ₂ O (4)	346	416	0.06	Violet

labelled +) and out of phase (state labelled -) combinations of the molecular excited states. The excitation energies E^+ and E^- of the Frenkel exciton states are split with respect to the energy of the isolated molecule E_0 , as a result of the excitonic interaction V^{exciton} .

The excitonic coupling can be shown to be composed of two dominant contributions:²⁴

$$V^{\text{exciton}} = V^{\text{Coulomb}} + V^{\text{Exchange}} \quad (1)$$

of which the first term shows a long range dependence which dominates the coupling between singlet excited states, while the second is a short range contribution which becomes relevant at short intermolecular distances.

The above discussion shows that the exciton coupling can be estimated in a supramolecular approach (V^{supra}) by computing the excitation energies E^+ and E^- ²⁵ and the difference $\Delta\epsilon$ between the excitation energies of the isolated molecules, when these are not identical (and assuming negligible polarization driven site energy splitting), from which the exciton coupling can be derived as

$$V^{\text{supra}} = \frac{1}{2} \sqrt{(E^+ - E^-)^2 - (\Delta\epsilon)^2} \quad (2)$$

We also estimated the Coulombic contribution to the exciton coupling according to the point dipole approximation (PDA):

$$V^{\text{PDA}} = \frac{1}{4\pi\epsilon_0} k \frac{|\mu_1| \cdot |\mu_2|}{r_{12}^3} \quad (3)$$

where k , the orientational factor, is expressed in terms of unitary vectors

$$k = (\check{\mu}_1 \cdot \check{\mu}_2) - 3(\check{\mu}_1 \cdot \check{r}_{12})(\check{\mu}_2 \cdot \check{r}_{12}) \quad (4)$$

and μ_1 and μ_2 are the transition dipole moments of the two molecules forming the dimer and r_{12} is their distance.

While the PDA approach is valid for distances larger than the molecular dimension and provides an estimate of the Coulombic term in the excitonic interaction, in the supramolecular approach both the Coulombic and exchange terms are included in the indirect evaluation of V^{supra} .^{25,26} In addition, in the supramolecular approach the Coulombic term is correctly estimated in contrast with the PDA approach where it is obtained by a truncated multipolar approximation.

The exciton interactions, computed with the two approaches outlined above and collected in Table 4, show the typical magnitudes reported for other conjugated chromophores in crystals.²⁷ According to the PDA approach, we can classify the dimers of the investigated crystals as J or H aggregates by considering the direction of the molecular transition dipole moments. For the NEaH chromophores and their

Table 4 TDHF/6-31+G* Computed excitonic interactions (with the PDA and supramolecular approaches) for the most relevant dimers of compounds 0–2

Dimer	PDA (cm ⁻¹)	Supramolecular (cm ⁻¹)	Compound
A	351	620	0
B	321	536	0
A	291	201	1
B	4	155	1
C	205	130	1
A	855	211	2
B	435	918	2



Fig. 14 Direction of the computed transition dipole moment for NEaH (left) and NEa (right).

anions, the transition dipole moment is directed along the short naphthalene molecular axis, as shown in Fig. 14.

Notably, the investigated dimer configurations of compounds 1 and 2 correspond to arrangements of the monomers typical for H aggregates²⁸ except for the dimer B of 2. In this latter case, the J character deduced according to the PDA approximation turns into H character when the less approximated supramolecular approach is considered. As for the dimers of compound 0, these can be classified as *non-planar transition dipoles* according to the PDA classification discussed in reference²⁸ and are neither J nor H pure aggregates. Inspection of Table 4 shows that very large variations occur when moving to the PDA approach to the supramolecular approach as a result of their different level of approximation. This is particularly evident for dimer B of compound 1 whose exciton coupling is almost zero, at PDA level, since the angle formed by the direction of the molecular transition dipole moments and the intermolecular distance vector (see Table S2†) is close to the limit angle of 54.7²⁸ which corresponds to zero excitonic interaction. Moving to the less approximated supramolecular approach leads to a non-negligible interaction as shown in Table 4. A similar drastic change in computed interactions concerns those of compound 2. Moving from the PDA to the supramolecular approach, the magnitudes of the interactions of the two investigated dimers exchange each other. Interestingly, however, this compound, among the three computationally investigated, is the one displaying the largest interactions for both approaches. We note that the two molecules forming the dimers are, in this case, identical and equivalent by symmetry, therefore the results from the supramolecular approach are deemed reliable. As a result of the comparably larger excitonic interactions, we expect in this case stronger photophysical changes: since the aggregation is of H type, a larger SS is generally expected. The tendency to form

excimers should also be considered in the discussion of the observed spectroscopic changes. However, the largest observed changes between absorption and emission for compound **2** can be reasonably accounted for by the largest computed excitonic interactions.

Conclusions

In this paper we have reported on the crystalline molecular salts formed by reaction of 2-(1,8-naphthalimido)ethanoic acid [NEaH] (**0**) with various cyclic amines, namely [DABCOH₂][NEa]₂ (**1**), [ABCOH][NEa]·4H₂O (**2**), [OH-ABCOH][NEa]·1.5H₂O (**3**), and [PIPH₂][NEa]₂·4H₂O (**4**). All solids have been structurally and thermally investigated by a combination of solid-state techniques, including differential scanning calorimetry (DSC), thermogravimetric analysis (TGA), single crystal and variable temperature powder X-ray diffraction (VT-XRPD). All compounds should be described as molecular salts and not as co-crystals, as in all cases proton transfer takes place from NEaH to the base; the difference between the two types of multicomponent crystals is, however, rather semantic and it has been amply demonstrated²⁹ that in hydrogen bonded systems there is almost a continuum of situations, also dependent on temperature, whereby the hydrogen is transferred from the acid to the base, and that the bulk physical properties of the materials (solubility, dissolution rates, melting point) do not seem to depend on the degree of proton transfer.

Upon heating, water loss is observed for all compounds, followed by formation of crystalline anhydrous phases (**2_anhyd**, **3_anhyd**, and **4_anhyd**), which revert back to their hydrate form upon cooling to room temperature.

Photoluminescence properties of solid **1**, **2**, **3**, and **4** have also been investigated and compared with those of **0**, both in solution and in the solid state. For all compounds fluorescence spectra in the solid state are red-shifted with respect to those in solution; luminescence in the solid state is observed at different wavelengths, from violet (*ca.* 420 nm for **1** and **4**) to green (*ca.* 490 nm for **2** and **3**) passing from blue (*ca.* 460 nm for **0**). These variations can be interpreted on the basis of the different intermolecular van der Waals, π - π and excitonic interactions amongst the naphthalimide moieties.

The modulation of excitonic interactions as a function of crystal packing has been computed with quantum-chemical methods. The largest excitonic interactions are indeed computed for compound **2** displaying the largest photophysical changes. Thus, the choice of the amine used as base/co-former has a marked effect on the supramolecular interactions formed in the solid state and results in a modification of the NEaH solid state fluorescence.

Work is in progress to further investigate and design the luminescent properties of multicomponent systems (salts and co-crystals) of luminescent dyes in the solid-state.

Synthesis of NEaH (**0**)

The 2-(1,8-naphthalimido)ethanoic acid was synthesized according to a previously reported procedure.^{11,30} To a

solution of glycine (0.55 g, 7.3 mmol) in H₂O (8 ml) 0.37 g (6.6 mmol) of solid KOH were added, and the solution was stirred for 20 minutes. Then 1.3 g (6.6 mmol) of naphthalene monoanhydride (NMa) suspended in *ca.* 25 mL of EtOH were added. The cream-coloured suspension was left under reflux for 6–8 h; the resulting clear solution was cooled to RT and concentrated HCl (37%) was added dropwise until a white precipitate was obtained. The product was recovered by filtration and washed with cold H₂O (5 × 2 mL) and with cold EtOH (5 × 2 mL). The solid obtained was dried overnight in a desiccator [yield = 76% (1.35 g, 5 mmol)]; it was then suspended in *ca.* 10 mL of methanol and boiled until a clear solution was obtained. Colourless, needle-shaped crystals of NEaH (identified by X-ray powder diffraction) grew from this solution in 24 h.

Synthesis of [DABCOH₂][NEa]₂ (**1**)

A suspension of NEaH (32.4 mg, 0.12 mmol) and DABCO (10.9 mg, 0.097 mmol) in *ca.* 10 mL of H₂O–EtOH 3:7 was boiled until a clear solution was obtained. Colourless, prism-like crystals grew from this solution in *ca.* 2 days.

Synthesis of [ABCOH][NEa]·4H₂O (**2**)

A suspension of NEaH (31.9 mg, 0.12 mmol) and ABCO (12.4 mg, 0.11 mmol) in *ca.* 10 mL of H₂O was boiled until a clear solution was obtained. Colourless, prism-like crystals grew from this solution in *ca.* 2 days.

Synthesis of [OH-ABCOH][NEa]·1.5H₂O (**3**)

A suspension of NEaH (29.6 mg, 0.11 mmol) and OH-ABCO (14 mg, 0.11 mmol) in *ca.* 10 mL of ethanol–H₂O 7:3 was boiled until a clear solution was obtained. Slow evaporation of this solution yielded a white powder. Colourless, prismatic crystals were obtained upon recrystallization of the powder from *n*-propanol.

Synthesis of [PIPH₂][NEa]₂·4H₂O (**4**)

A suspension of NEaH (60.8 mg, 0.22 mmol) and PIP (9.7 mg, 0.11 mmol) in *ca.* 10 mL of ethanol–H₂O 6:4 was boiled until a clear solution was obtained. Slow evaporation of this solution yielded a white powder. Colourless, prismatic crystals were obtained upon recrystallization of the powder from *n*-propanol.

Syntheses in the solid state

In the solid-state reactions NEaH was manually ground in an agate mortar for *ca.* 10 min with DABCO, ABCO, OHABCO, or PIP in 1:1 molar ratio. In all the kneading experiments a few drops of solvent (H₂O or EtOH) were added to the grinding mixture. Formation of the solid products **1**, **2**, **3** and **4** was confirmed by comparison of the experimental XRPD patterns with those calculated on the basis of single crystal structures.

Crystal structure determination

Single-crystal data for all compounds were collected at RT on an Oxford X'Calibur S CCD diffractometer equipped with a graphite monochromator (Mo-K α radiation, $\lambda = 0.71073$ Å). Data collection and refinement details are listed in Table S5.† All non-hydrogen atoms were refined anisotropically; H_{OH} and H_{NH} atoms were either directly located or added in calculated positions; H_{CH} atoms for all compounds were added in calculated positions and refined riding on their respective carbon atoms. SHELX97^{31a} was used for structure solution and refinement on F^2 . The program PLATON^{31b} was used to calculate hydrogen bonding interactions. CYLview,^{31c} Mercury^{31d} and Schakal99^{31e} were used for molecular graphics. CCDC 941379–941382† contain the supplementary crystallographic data for this paper.

Powder diffraction measurements

X-ray powder diffractograms in the 2θ range 5–40° (step size, 0.02°; time per step, 20 s; 0.04 rad s⁻¹ s⁻¹; $V \times A$ 40 × 40) were collected in Bragg–Brentano geometry on a Panalytical X'Pert PRO automated diffractometer equipped with an X'Celerator detector, using Cu K α radiation without a monochromator. The program Mercury^{31d} was used for calculation of X-ray powder patterns on the basis of single crystal data. The identity between bulk materials and single crystals was always verified by comparing calculated and experimental powder diffraction patterns (see Fig. S1†). For variable temperature experiments the diffractometer was equipped with an Anton Paar TTK 450 system for measurements at controlled temperature. All data were collected in open air.

Differential scanning calorimetry (DSC)

Calorimetric measurements were performed with a Perkin-Elmer DSC-7 equipped with a PII intracooler. Temperature and enthalpy calibrations were performed using high-purity standards (*n*-decane, benzene and indium). Heating of the aluminium open pans containing the samples (3–5 mg) was carried out at 5 °C min⁻¹ in the temperature range 40–350 °C.

Thermogravimetric analysis (TGA)

Thermogravimetric analyses were performed with a Perkin-Elmer TGA-7. Heating was performed in a nitrogen flow (20 cm³ min⁻¹) using a platinum crucible at the rate of 5 °C min⁻¹ up to decomposition. The sample weights were in the range 5–10 mg.

Photophysics

Solvents used for photophysical determinations were of spectroscopic grade (C. Erba). UV-Vis absorption spectra were recorded at room-temperature with a Perkin-Elmer Lambda 45 spectrophotometer. Quartz cuvettes with optical path length of 1 cm were used. Fluorescence spectra were recorded with a Perkin-Elmer LS 50 spectrofluorimeter, the uncertainty

on the band maxima is 2 nm. Luminescence quantum yields were determined using air equilibrated solutions of naphthalene in cyclohexane ($\Phi = 0.036$).

All measurements on solid samples were performed on finely ground powder placed inside two quartz slides (sandwich mode). Emission and excitation spectra of solid samples were acquired on a Perkin-Elmer LS 50 spectrofluorimeter; the uncertainty on the band maxima is 2 nm.

Absolute photoluminescence quantum yields were measured according to the method of deMello³² by using a custom designed integrating sphere inside a SPEX Fluorolog fluorometer and checking the precision of the measurements with reference samples in the same experimental setup.³³

Computational details

The ground state and excited state potential energy surfaces were computed at both CAM-B3LYP/6-31+G* and B3LYP/6-31+G* levels of theory. The basis set was chosen in view of the excited state switching predicted for basis sets not including diffuse functions (see ref. 34). The computed optimized geometries of the ground and excited states of NEaH are collected in Fig. S4.†

Transition dipole moments were evaluated with time dependent (TD) DFT calculations carried out on the molecules forming the dimers. The TDHF/6-31+G* level of theory was employed in this case and for the following evaluation with the supramolecular approach to avoid mixing between Frenkel and charge transfer exciton states as already pointed out in previous studies.³⁵

In the supramolecular approach the excitonic interaction is indirectly estimated by the excitation energies of the two excitonic states computed for molecular dimers. Therefore the following steps have been followed: (a) calculation of excitation energies for molecular dimers, (b) identification of the two Frenkel excitations of the dimer and (c) evaluation of the exciton coupling V . In keeping with their molecular salts nature, when evaluating exciton interactions with PDA and supramolecular approaches the anionic form, [NEa]⁻, was considered for compounds 1 and 2.

Acknowledgements

We thank the University of Bologna and MIUR for financial support. We thank Dr. Massimo Sgarzi for photophysics measurements in solution.

Notes and references

- (a) G. R. Desiraju in *Crystal Engineering: The Design of Organic Solids*, ed. G. R. Desiraju. Elsevier, Amsterdam, 1989; (b) D. Braga, F. Grepioni and A. G. Orpen, in *Crystal Engineering: from Molecules and Crystal to Materials*, ed. D. Braga, F. Grepioni and A. G. Orpen, Kluwer Academic Publishers, Dordrecht, 1999; (c) G. R. Desiraju, *J. Chem. Sci.*,

- 2010, 122, 667–675; (d) D. Braga, F. Grepioni and L. Maini, *Chem. Commun.*, 2010, 46, 6232–6242; (e) C. B. Aakeröy, N. R. Champness and C. Janiak, *CrystEngComm*, 2010, 12, 22–43.
- 2 (a) M. Nagarathinam, A. M. P. Peedikakkal and J. J. Vittal, *Chem. Commun.*, 2008, 5277–5288; (b) L. R. MacGillivray, *J. Org. Chem.*, 2008, 73, 3311–3317; (c) Y. Sonoda, *Molecules*, 2011, 16, 119–148; (d) D. Braga, S. d'Agostino and F. Grepioni, *Cryst. Growth Des.*, 2012, 12, 4880–4889.
- 3 (a) V. Andre, M. T. Duarte, D. Braga and F. Grepioni, *Cryst. Growth Des.*, 2012, 12, 3082–3090. D. Braga, F. Grepioni, L. Maini, D. Capucci, S. Nanna, J. Wouters, L. Aerts and L. Quéré, *Chem. Commun.*, 2012, 48, 8219–8221.
- 4 (a) J. D. Wuest, *Nat. Chem.*, 2012, 4, 74–75; (b) G.-G. Hou, H.-J. Zhao, J.-F. Sun, D. Lin, X.-P. Dai, J.-T. Han and H. Zhao, *CrystEngComm*, 2013, 15, 577–585; (c) Y. Abe, S. Karasawa and N. Koga, *Chem.–Eur. J.*, 2012, 18, 15038–15048; (d) L. Quan, Y. Chen, X.-J. Lv and W.-F. Fu, *Chem.–Eur. J.*, 2012, 18, 14599–14604; (e) S. Chen, N. Chen, Y. L. Yan, T. Liu, Y. Yu, Y. Li, H. Liu, Y. S. Zhao and Y. Li, *Chem. Commun.*, 2012, 48, 9011–9013; (f) D. Yan, A. Delori, G. O. Lloyd, B. Patel, T. Frišćić, G. M. Day, D.-K. Bučar, W. Jones, J. Lu, M. Wei, D. G. Evans and X. Duan, *CrystEngComm*, 2012, 14, 5121–5123; (g) S. Philip Anthony, S. Varughese and S. M. Draper, *J. Phys. Org. Chem.*, 2010, 23, 1074–1079; (h) T. Hinoue, Y. Shigenoi, M. Sugino, Y. Mizobe, I. Hisaki, M. Miyata and N. Tohnai, *Chem.–Eur. J.*, 2012, 18, 4634–4643; (i) D. Yan, A. Delori, G. O. Lloyd, T. Frišćić, G. M. Day, W. Jones, J. Lu, M. Wei, D. G. Evans and X. Duan, *Angew. Chem., Int. Ed.*, 2011, 50, 12483–12486.
- 5 (a) O. Bolton, K. Lee, H.-J. Kim, K. Y. Lin and J. Kim, *Nat. Chem.*, 2011, 3, 205–210; (b) X. P., H. Wang, X. R. Zhao and W. J. Jin, *CrystEngComm*, 2013, 15, 2722–2730; (c) H. Y. Gao, X. R. Zhao, H. Wang, X. Pang and W. J. Jin, *Cryst. Growth Des.*, 2012, 12, 4377–4387.
- 6 P. Bamfield and M. G. Hutchings in *Chromic Phenomena Technological Applications of Colour Chemistry*, 2nd edn, ed. P. Bamfield and M. G. Hutchings, Royal Society of Chemistry, Cambridge, 2010.
- 7 (a) R. H. Friend, R. W. Gymer, A. B. Holmes, J. H. Burroughes, R. N. Marks, C. Taliani, D. D. C. Bradley, D. A. Dos Santos, J. L. Brédas, M. Lögdlund and W. R. Salaneck, *Nature*, 1999, 397, 121–128; (b) C. A. Strassert, C. Chien, M. D. G. Lopez, D. Kourkoulos, D. Hertel, K. Meerholz and L. De Cola, *Angew. Chem.*, 2011, 123, 976–980; (c) C. A. Strassert, C. Chien, M. D. G. Lopez, D. Kourkoulos, D. Hertel, K. Meerholz and L. De Cola, *Angew. Chem., Int. Ed.*, 2011, 50, 946–950; (d) J. You, G. Li, R. Wang, Q. Nie, Z. Wang and J. Li, *Phys. Chem. Chem. Phys.*, 2011, 13, 17825–17830; (e) K. Watanabe, T. Sakamoto, M. Taguchi, M. Fujiki and T. Nakano, *Chem. Commun.*, 2011, 47, 10996–10998.
- 8 (a) D. Kolosov, V. Adamovich, P. Djurovich, M. E. Thompson and C. Adachi, *J. Am. Chem. Soc.*, 2002, 124, 9945–9954; (b) F. Cacialli, R. H. Friend, C. M. Bouche, P. Le Barny, H. Facoetti, F. Soyer and P. Robin, *J. Appl. Phys.*, 1998, 83, 2343–2356.
- 9 (a) T. Peters and M. J. Bide, *Dyes Pigm.*, 1985, 6, 349–375; (b) T. Konstantinova, P. Meallier and I. Grabtchev, *Dyes Pigm.*, 1993, 22, 191–198.
- 10 (a) J. Gan, K. Chen, C.-P. Chang and H. Tian, *Dyes Pigm.*, 2003, 57, 21–28; (b) Z. Jin, X.-B. Zhang, D.-X. Xie, Y.-J. Gong, J. Zhang, X. Chen, G.-L. Shen and R.-Q. Yu, *Anal. Chem.*, 2010, 82, 6343–6346; (c) T. Gunnlaugsson, P. E. Kruger, P. Jensen, J. Tierney, H. D. P. Ali and G. M. Hussey, *J. Org. Chem.*, 2005, 70, 10875–10878; (d) I. Grabchev, I. Moneva, V. Bojinov and S. Guittonneau, *J. Mater. Chem.*, 2000, 10, 1291–1296; (e) V. F. Pais, P. Remon, D. Collado, J. Andeasson, E. Perez-Inestrosa and U. Pischel, *Org. Lett.*, 2011, 13(20), 5572–5575.
- 11 D. L. Reger, A. Debreczeni, J. J. Horger and M. D. Smith, *Cryst. Growth Des.*, 2011, 11, 4068–4079.
- 12 (a) D. Braga, L. Maini and F. Grepioni, *Chem. Soc. Rev.*, 2013, 42, 7638–7648; (b) D. Braga, S. d'Agostino, E. Dichiarante, L. Maini and F. Grepioni, *Chem.–Asian J.*, 2011, 6, 2214–2223; (c) S. L. James, C. J. Adams, C. Bolm, D. Braga, P. Collier, T. Frišćić, F. Grepioni, K. D. M. Harris, G. Hyett, W. Jones, A. Krebs, J. Mack, L. Maini, A. G. Orpen, I. P. Parkin, W. C. Shearouse, J. W. Steed and D. C. Waddell, *Chem. Soc. Rev.*, 2012, 41, 413–447.
- 13 (a) D. Braga and F. Grepioni, *Acc. Chem. Res.*, 2000, 33, 601–608; (b) P. Gilli and G. Gilli, in *Supramolecular Chemistry: From Molecules to Nanomaterials*, ed. P. A. Gale and J. W. Steed, WILEY-VCH, Weinheim, 2012, pp. 2829–2867.
- 14 (a) L. Infantes and S. Motherwell, *CrystEngComm*, 2002, 4, 454–461; (b) L. Infantes, J. Chisholm and S. Motherwell, *CrystEngComm*, 2003, 5, 480–486; (c) M. Mascal, L. Infantes and J. Chisholm, *Angew. Chem., Int. Ed.*, 2006, 45, 32–36.
- 15 (a) S. M. Alexiou, V. Tychopoulos, S. Ghorbanian, J. H. P. Tyman, R. G. Brown and P. I. Brittain, *J. Chem. Soc., Perkin Trans. 2*, 1990, 837–842; (b) H. Cao, V. Chang, R. Hernandez and M. D. Heagy, *J. Org. Chem.*, 2005, 70, 4929–4934.
- 16 V. Wintgens, P. Valat, J. Kossanyi, L. Biczok, A. Demeter and T. Berces, *J. Chem. Soc., Faraday Trans.*, 1994, 90(3), 411–421.
- 17 (a) P. Berci, V. G. Toscano and M. J. Politi, *J. Photochem. Photobiol., A*, 1988, 43(1), 51–58; (b) K. Matsubayashi and Y. Kubo, *J. Org. Chem.*, 2008, 73(13), 4915–4919.
- 18 (a) L. Biczok, T. Berces and H. Linschitz, *J. Am. Chem. Soc.*, 1997, 119(45), 11071–11077; (b) O. V. Prezhdo, B. V. Uspenskii, V. V. Prezhdo, W. Boszczyk and V. B. Distanov, *Dyes Pigm.*, 2007, 72(1), 42–46.
- 19 Y. Mizobe, T. Hinoue, A. Yamamoto, I. Hisaki, M. Miyata, Y. Hasegawa and N. Tohnai, *Chem.–Eur. J.*, 2009, 15(33), 8175–8184.
- 20 (a) T. C. Barros, P. Berci, V. G. Toscano and M. J. Politi, *J. Photochem. Photobiol., A*, 1995, 89(2), 141–146; (b) D. W. Cho, M. Fujitsuka, K. H. Choi, M. J. Park, U. C. Yoon and T. Majima, *J. Phys. Chem. B*, 2006, 110(10), 4576–4582; (c) D. W. Cho, Fujitsuka, M. A. Sugimoto and T. Majima, *J. Phys. Chem. A*, 2008, 112(31), 7208–7213.
- 21 F. C. Spano, *Acc. Chem. Res.*, 2010, 43, 429–439.

- 22 J.-L. Bredas, D. Beljonne, V. Coropceanu and J. Cornil, *Chem. Rev.*, 2004, **104**, 4971–5003.
- 23 (a) S. Di Motta, M. Siracusa and F. Negri, *J. Phys. Chem. C*, 2011, **115**, 20754–20764; (b) E. Di Donato, R. P. Fornari, S. Di Motta, Y. Li, Z. Wang and F. Negri, *J. Phys. Chem. B*, 2010, **114**, 5327–5334; (c) S. Di Motta, E. Di Donato, F. Negri, G. Orlandi, D. Fazzi and C. Castiglioni, *J. Am. Chem. Soc.*, 2009, **131**, 6591–6598.
- 24 G. D. Scholes and K. P. Ghiggino, *J. Phys. Chem.*, 1994, **98**, 4580–4590.
- 25 R. Fink, J. Pfister, A. Schneider, H. Zhao and B. Engels, *Chem. Phys.*, 2008, **343**, 353–361.
- 26 D. Beljonne, J. Cornil, R. Silbey, P. Millié and J.-L. Bredas, *J. Chem. Phys.*, 2000, **112**, 4749–4758.
- 27 D. Fazzi, C. Quarti and M. Del Zoppo, *Phys. Chem. Chem. Phys.*, 2011, **13**, 18615–18625.
- 28 M. Kasha, H. R. Rawls and M. Ashraf El-Bayoumi, *Pure Appl. Chem.*, 1965, **11**, 371–392.
- 29 (a) D. Braga, L. Maini, G. De Sanctis, K. Rubini, F. Grepioni, M. R. Chierotti and R. Gobetto, *Chem.–Eur. J.*, 2003, **9**, 5538–5548; (b) S. Childs, G. P. Stahly and A. Park, *Mol. Pharmaceutics*, 2007, **4**, 323–338.
- 30 D. L. Reger, J. J. Horger, A. Debreczeni and M. D. Smith, *Inorg. Chem.*, 2011, **50**, 10225–10240.
- 31 (a) G. M. Sheldrick, *SHELX97, Program for Crystal Structure Determination*, University of Göttingen. Göttingen, Germany, 1997; (b) A. L. Spek, *PLATON Acta Crystallogr., Sect. A: Found. Crystallogr.*, 1990, **46**, C34; (c) C. Y. Legault, *CYLview, 1.0b*, Université de Sherbrooke, Sherbrooke, Canada, 2009; (d) C. F. Macrae, I. J. Bruno, J. A. Chisholm, P. R. Edgington, P. McCabe, E. Pidcock, L. Rodriguez-Monge, R. Taylor, J. van de Streek and P. A. J. Wood, *J. Appl. Crystallogr.*, 2008, **41**, 466–470; (e) E. Keller, *SCHAKAL99*, Graphical Representation of Molecular Models, University of Freiburg, Freiburg, Germany, 1999.
- 32 J. C. deMello, H. F. Wittmann and R. H. Friend, *Adv. Mater.*, 1997, **9**, 230–232.
- 33 More information about the theory and practice of integrating spheres can be found in the Technical Notes “A Guide to Integrating Sphere, Theory and Applications”, available at <http://www.labsphere.com>, and “Integrating Sphere, Design and Applications”, available at <http://www.sphereoptics.com>.
- 34 D. Jacquemin, E. A. Perpete, G. Scalmani, M. J. Frisch, I. Ciofini and C. Adamo, *Chem. Phys. Lett.*, 2007, **448**, 3–6.
- 35 R. F. Fink, J. Pfister, H. M. Zhao and B. Engels, *Chem. Phys.*, 2008, **346**, 275–285.